

Switching of sub- μm sized, antiferromagnetically coupled CoFeB/Ru/CoFeB trilayers

N. Wiese*

Siemens AG, Corporate Technology, Paul-Gossen-Str. 100, 91052 Erlangen, Germany and
University of Bielefeld, Nano Device Group, Universitätsstr. 25, 33615 Bielefeld, Germany

T. Dimopoulos, M. Rührig, and J. Wecker

Siemens AG, Corporate Technology, Paul-Gossen-Str. 100, 91052 Erlangen, Germany

G. Reiss

University of Bielefeld, Nano Device Group, Universitätsstr. 25, 33615 Bielefeld, Germany

(Dated: May 24, 2019)

This work reports on the magnetic reversal of sub- μm sized elements consisting of an CoFeB/Ru/CoFeB artificial ferrimagnet (AFi). The elements were patterned into ellipses having a width of approximately 250 to 270nm and a varying aspect ratio between 1.3 and 8. The coercivity was found to decrease with an increasing imbalance of the magnetic moment of the two antiferromagnetically coupled layers and is therefore strongly affected by an increase of effective anisotropy due to the antiferromagnetic coupling of the two layers. With respect to a single layer of amorphous CoFeB, patterned in comparable elements, the AFi has an increased coercivity. Switching asteroids comparable to single layers were only observed for samples with a high net moment.

PACS numbers: 75.75.+a,75.50.Kj

I. INTRODUCTION

Magnetic tunnel junctions (MTJ) have gained considerable interest in recent years due to their high potential in various applications, e.g. as reads heads (1), angle (2) or strain sensors (3) and as programmable resistance in data storage (MRAM) (4) or even magnetic logic devices (5).

The underlying concept is a spin valve consisting of a hard magnetic reference electrode separated from the soft magnetic sense or storage layer by a tunnel barrier like

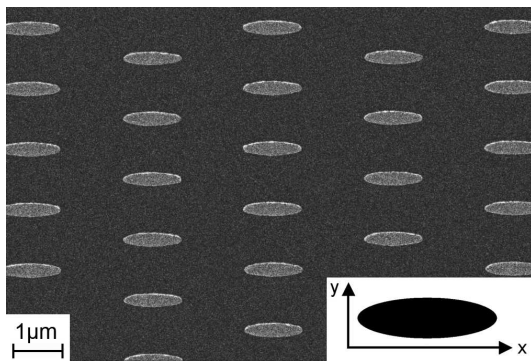


FIG. 1 SEM images of one of the arrays of sample D, showing ellipses with the size of $0.27\mu\text{m} \times 1.18\mu\text{m}$.

Al_2O_3 . The reference layer usually is an artificial ferrimagnet (AFi) exchange biased by a natural antiferromagnet, in which the AFi consists of two ferromagnetic layers coupled antiparallel via a thin non-magnetic spacer. For the soft electrode, mostly single layers of polycrystalline material, e.g NiFe and CoFe, have been used (6). Recently, soft electrodes of polycrystalline AFis, based on ferromagnetic materials like CoFe and NiFe, have been investigated. They show a further reduction of the stray field due to the reduced net moment, smaller switching field distribution (7) and an easier establishment of a single domain structure in patterned elements with small aspect ratio (8).

Additionally, the concept of an AFi allows one to further adjust the magnetic properties of the soft layer. Compared to the coercivity of a continuous single layer, H_c^{SL} , the coercivity of the AFi, H_c^{AFi} , is enhanced by a factor Q :

$$H_c^{\text{AFi}} = Q \cdot H_c^{\text{SL}} \quad \text{with} \quad Q = \frac{M_1 t_1 + M_2 t_2}{M_1 t_1 - M_2 t_2} \quad (1)$$

where M_1, M_2 and t_1, t_2 are the saturation magnetization and the thickness of the two composite ferromagnetic layers.(9) As shown before for unpatterned AFi films consisting of two amorphous, ferromagnetic CoFeB layers, separated by a thin Ru spacer, the coercivity can be tailored in a wide range and is approximately by a factor of nine smaller than in systems of polycrystalline CoFe/Ru/CoFe.(10) Furthermore the coupling of the amorphous CoFeB-AFi shows an oscillating behavior in dependence of the thickness of the nonmagnetic Ru

*Electronic Mail: mail@nilswiese.de

TABLE I Investigated samples and parameters extracted from the AGM measurements of the unpatterned layer systems.

| sample | system | Q_{meas} | H_{sat} | J |
|--------|-------------------------------|-------------------|----------------------|-------|
| | | [kA/m] | [mJ/m ²] | |
| A | CoFeB 3.5 / Ru 0.95 / CoFeB 3 | 7.7 | 29.8 | -0.06 |
| B | CoFeB 4.0 / Ru 0.95 / CoFeB 3 | 5.1 | 26.3 | -0.06 |
| C | CoFeB 4.5 / Ru 0.95 / CoFeB 3 | 3.7 | 23.9 | -0.06 |
| D | CoFeB 4 | | | |

spacer and achieves a coupling strength of the order of -0.1mJ/m^2 at the second antiferromagnetic maximum, which is about a factor of ten smaller than in polycrystalline CoFe/Ru/CoFe trilayers.(11)

It was the purpose of this study to investigate the switching behavior of the amorphous CoFeB-AFi at sub- μm sizes, where additional shape anisotropy and the magnetostatic edge coupling have to be taken into account. These contributions lead to an *effective anisotropy* which is for patterned elements different from the anisotropy of continuous films (eqn. 1).

As the amorphous alloy we chose Co₆₀Fe₂₀B₂₀ due to a high tunnel magnetoresistance (TMR) (12) and an enhanced temperature stability of the TMR (13). A thin Ru spacer was used to mediate the coupling between the two ferromagnetic layers of the AFi.

II. EXPERIMENTAL

Samples have been deposited by magnetron sputtering on thermally oxidized SiO₂ wafers at a base pressure of $5 \cdot 10^{-8}$ mbar. A magnetic field of approximately 4 kA/m was applied during deposition in order to induce the easy axis in the magnetic layers. The AFi was grown on a 1.2 nm thick Al layer, oxidized in an Ar/O₂ plasma for 0.8 min without breaking the vacuum, to have similar growth conditions as in a MTJ. In order to investigate the switching behavior in dependence on the Q-value, three different samples have been prepared where the thickness of the ferromagnetic layer in contact with the Al₂O₃ layer, and thus the net magnetic moment, has been varied (see table I, samples A to C). Additional a single CoFeB layers with a thickness of 4 nm (sample D) has been deposited for comparison. All samples were capped with a Ta layer to protect the multilayers from oxidation.

The samples have been patterned by a single step e-beam lithography and Ar-ion etching process. For lithography a positive e-beam resist was used, leading to patterns with a small edge roughness and high reproducibility across the whole array. On each sample different arrays of ellipses with a nominal width, w , of 250nm and varying length, ℓ , have been defined, leading to different aspect ratios, $u = \ell/w$, between 1.3 and 8. The lateral distances have been chosen three times the dimension of

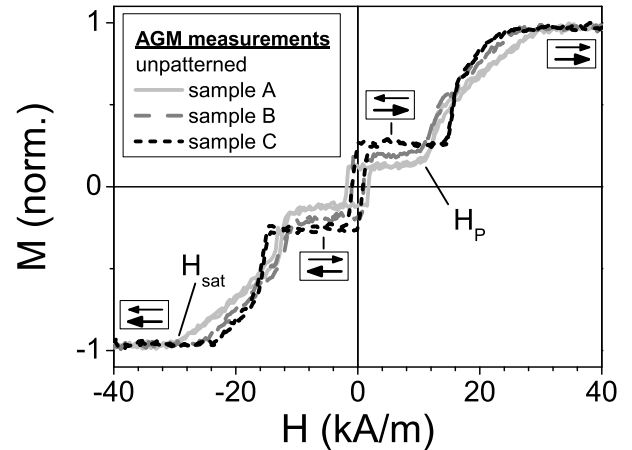


FIG. 2 Magnetization loops of unpatterned samples taken by AGM, showing a well established coupling for all AFi samples. The saturation field, H_{sat} , and the plateau field, H_p , are indicated for sample A.

the elements, and therefore a dipolar coupling between the individual ellipses of an array can be neglected.(14) Each of the arrays had the dimension of $25 \times 25\mu\text{m}^2$. After the arrays have been coated by a Ta layer of appropriate thickness (ranging from 8 to 15nm), the capping was removed in a lift-off process in a bath of solvent under application of ultrasonic agitation. During etching with a $80\text{ }\mu\text{A/cm}^2$ Ar ion current the samples were tilted by approximately 30 degrees and rotated to obtain a uniform etch profile over the sample. The etching depth was monitored by a secondary ion mass spectrometer (SIMS) attached to the etching facility.

The sizes and the uniformity of all patterns have been characterized by scanning electron microscopy (SEM) after the patterning process. The SEM image in figure 1 shows one of the arrays of sample D with ellipses in the size of $0.27\mu\text{m} \times 1.18\mu\text{m}$, confirming the high uniformity of the patterns. The width for samples with small aspect ratios ($u = \ell/w < 5$) varied between 250 and 270nm. Due to a tendency of over-exposure, ellipses with larger aspect ratios show a slightly larger widths of approximately 300nm.

After patterning all samples have been field annealed for 20min. at 150°C and 475kA/m applied parallel to the long axis of the ellipses using a vacuum annealing furnace. Magnetization loops of all arrays have been taken by a commercial magneto-optical Kerr effect magnetometer (MOKE) with a typical spot diameter of $4\mu\text{m}$.(15)

III. RESULTS AND DISCUSSION

A room temperature magnetization curve, $M(H)$, of the antiferromagnetically (AF) coupled systems is shown in figure 2. From the $M(H)$ loops, obtained by alternating gradient field magnetometry (AGM), one can extract the saturation field, H_{sat} , the total, $m_{\text{tot}} = m_1 + m_2$,

and the net magnetic moment, $m_{\text{net}} = m_1 - m_2$, allowing to calculate the measured Q -value, $Q_{\text{meas}} = m_{\text{tot}}/m_{\text{net}}$, the individual magnetization of the layers, $m_{1,2}$, and the coupling energy (9)

$$J = -\mu_0 H_{\text{sat}} \frac{m_1 m_2}{m_1 + m_2} \quad (2)$$

The coupling is -0.06mJ/m^2 for all investigated AFi samples. The values are in accordance to the oscillating coupling in dependence on the Ru spacer thickness around the second antiferromagnetic maximum as presented elsewhere.(11) The measured Q -values vary between 3.7 and 7.7 for the investigated AFi samples, and are significantly smaller than the Q value, Q_{nom} , calculated from the nominal thickness of the ferromagnetic layers. This discrepancy is supposed to result from a thicker magnetically dead layer of the upper CoFeB layer in comparison to the bottom layer. Since the samples are well protected from oxidation, as confirmed by Auger depth profiling, this would indicate a stronger intermixing of the upper CoFeB interfaces. All data extracted from the AGM measurements are given in table I.

Figure 3 shows the magnetization loops of patterned arrays of all AFi samples as obtained by MOKE measurements. The strong AF coupling is maintained after the patterning and annealing steps. Additionally, the saturation field is increasing with decreasing aspect ratio (i.e. length or size) of the ellipses, due to an increase in stray field coupling between the layers within the AFi system. For large aspect ratios H_{sat} achieves the values of the unpatterned samples.

The saturation field can be expressed by two contributions, one originating from the antiferromagnetic interlayer coupling, the other resulting from the stray field coupling. Whereas the first should depend on $-\frac{J}{\mu_0} \frac{m_1 + m_2}{m_1 m_2}$, as derived from eqn. 2, the latter should depend on $\mu_0 M_s \frac{t_{\text{tot}}}{w} n_x$,(16) where t_{tot} is the total thickness of the AFi. The second contribution only depends on the demagnetization factor n_x , since the y -components in case of an AF coupled system are compensated for external fields larger than the plateau field, H_p . Since the width of the elements was held constant for the investigated samples, the dependence of H_{sat} on the sample geometry is only given by the demagnetization factor(17)

$$n_x = \frac{u}{2} \int_0^\infty \frac{ds}{(u^2 + s) \cdot \sqrt{(u^2 + s)(1 + s)}} \quad (3)$$

This model is fitted to the measured data as shown in figure 4(a). The fitting shows a high accordance between the experimental data and the model, thus verifying the dependence of the saturation field on n_x for small aspect ratios. From the fitting parameters one can further extract the saturation field for an infinite elongated ellipse to 28.6 kA/m for sample A, 24.2 kA/m for sample B and 22.8 kA/m for sample C, respectively. These values are in good agreement to the measured saturation fields at the unpatterned AFi samples given by the interlayer coupling (see table I).

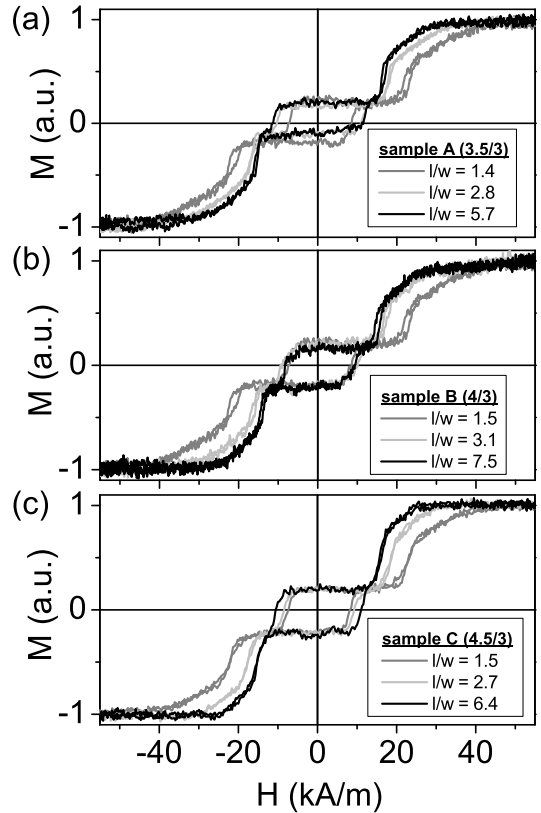


FIG. 3 Major magnetization loops measured by MOKE of some of the patterned arrays, showing a well established coupling and $H_p > H_c$ for all samples.

For external fields smaller than H_p , the AF coupling remains stable. As can be seen from figure 3, the AFi should reverse its magnetization like a single layer sample with a reduced net moment and enhanced effective anisotropy. Therefore it is possible to measure minor magnetization loops in a small field window (± 10 to ± 15 kA/m, depending on H_p of the sample) and extract the coercivity, H_c , of the arrays (see figure 4(b)).

For small aspect ratios ($u < 4$), H_c increases with u by approximately 3.5 kA/m and remains constant for large aspect ratios (see figure 4(b)). The slight decrease in coercivity for the largest aspect ratios is most likely attributed to the slightly larger width of the ellipses. This behavior of the coercivity vs. aspect ratio holds also for the single layer sample. The increase of H_c for small aspect ratios is caused by the increase in shape anisotropy, which for an ellipse is given by(16)

$$H_c = 4\pi M_s \frac{t_{\text{net}}}{w} (n_y - n_x) \quad (4)$$

where the demagnetization factor ($n_y - n_x$) depends on the aspect ratio. Therefore the experimental results of figure 4 (b) are in qualitative accordance with the $(n_y - n_x)$ dependence on aspect ratio (see figure 4(c)). Deviations from the calculated dependence for large aspect ratios are likely to result from micromagnetic differ-

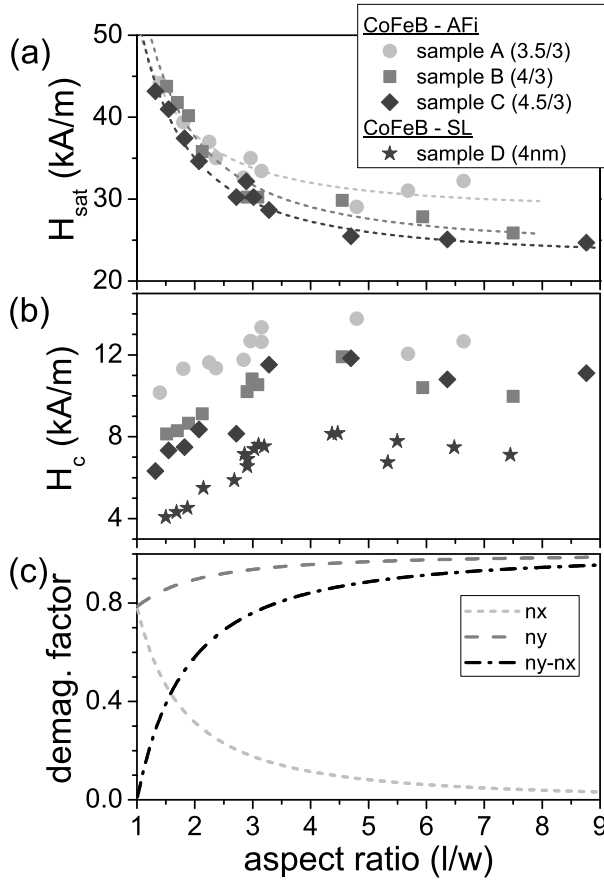


FIG. 4 (a) Saturation field, H_{sat} , and (b) coercivity, H_c , of patterned samples vs. the aspect ratio $u = \ell/w$. The width of approximately 250 to 270nm was kept constant for all investigated samples. The dashed lines in (a) represent a fit with a function proportional to the demagnetization factor n_x . (c) Numerical calculated demagnetization factors for ellipses against the aspect ratio.

ences: Small elements are stabilized by a non vanishing stray field, arising from the magnetic poles of the elements. These stray fields stabilize the overall magnetization of the elements, so that the reversal can be more accurately approximated by a single domain mechanism. For large aspect ratios the magnetic poles are larger separated, thus minimizing the stray field coupling and as a result a nucleation driven magnetization reversal, most likely initiated by edge domains, is more favourable, leading to a almost constant coercivity.(18)

Unlike elliptic elements with a single ferromagnetic layer, the coercivity of the patterned AFi samples does not scale proportional to the net magnetic moment. With higher net moment, the coercivity is *decreasing*, but remaining always larger than for elements of a 4nm thick single layer. The reason is a superposition of the effective anisotropy due to the AF coupling ($\sim m_{\text{tot}}/m_{\text{net}}$), as expressed by eqn. 1 for the unpatterned films, and the dependence of coercivity on the net magnetic moment as described by eqn. 4 ($\sim m_{\text{net}}(n_y - n_x)/w$). Overall

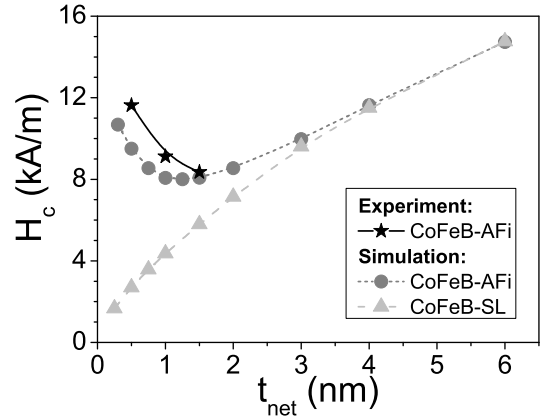


FIG. 5 Experimental and calculated dependence of coercivity, H_c , on the net thickness, t_{net} , of the AFi and a single layer, respectively. The experimental data points are for elliptical shaped elements with the dimension of 250nm \times 520nm, the simulated data are evaluated for the same sample geometry. Lines are guides to the eye.

the influence of the AF coupling is dominating for the investigated CoFeB AFis and the coercivity is increased by approximately a factor of 1.4 when decreasing the net thickness of the AFi, and therefore the net moment, from 1.5 to 0.5nm.

The dependence of coercivity on the net thickness, $t_{\text{net}} = t_2 - t_1$, of the AFi and for single layer samples with layer thicknesses of $t = t_{\text{net}}$ have been simulated within a micromagnetic model using Landau-Lifshitz-Gilbert equations (see figure 5).(19) For the simulation of the AFis the thickness of the second FM layer, t_2 , was varied between 3.5 and 6nm, whereas the thickness of the first FM layer was kept fixed to $t_1 = 3$ nm, and the thickness of the nonmagnetic spacer was chosen to 1nm. The saturation moment of the FM layers were assumed to $M_s = 860\text{emu}/\text{cm}^3$, the uniaxial anisotropy to $K_u = 2.4 \cdot 10^3\text{erg}/\text{cm}^3$, the exchange stiffness constant to $A = 1.05 \cdot 10^{-6}\text{erg}/\text{cm}$ and for the AF coupling constant to $J = -0.004 \cdot 10^{-6}\text{erg}/\text{cm}$. The coercivity of the simulated elliptic AFi elements of 250nm \times 520nm decreases with net thickness for $t_{\text{net}} \leq 1.5$ nm, and increases for larger t_{net} , asymptotically reaching the values of the single layer coercivity. The experimental data of the AFi arrays with the same geometry show a similar behavior, therefore verifying the above described model for the samples under study.

Figure 6 shows the bias field dependence of the coercivity for samples patterned with an aspect ratio of $u \approx 2.2$. Due to the increase of effective anisotropy with the Q-value (and therefore basically with the inverse net magnetic moment), the asteroid gets stretched along the hard axis field. If used in a conventional writing scheme as a soft magnetic electrode for applications like MRAM or magnetic logic, the broad asteroid shape of the AFi storage layer cells limits the choice of Q-value due to field limitations, reducing the proposed advantages of an

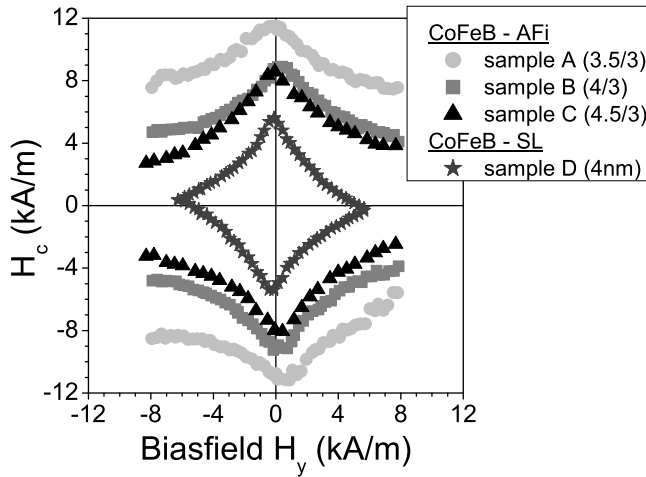


FIG. 6 Bias field dependence of the coercivity for all investigated film systems with an aspect ratio $u \approx 2.2$, illustrating also the gain in effective anisotropy by introduction of the antiferromagnetic coupling and the strong influence of the increased Q-value on the anisotropy of the system.

AFi structure as reported by others.(7; 8)

IV. CONCLUSION

The AFi based on an amorphous CoFeB alloy shows a strong increase in the effective anisotropy due to the AF coupling, mediated by a thin Ru interlayer and by the stray field coupling, respectively. This is reflected by a higher coercivity and an increase of the asteroid width compared to a single CoFeB layer. The dependence of the switching field on the net magnetic moment can not be explicitly explained within the model that considers the AFi as a rigid ferromagnetic layer with a reduced moment. One has further to take into account the increase of effective anisotropy, which basically scales with the inverse net moment for the investigated combinations of layer thicknesses. This last factor appears to be dominating in the system under study and leads to the decrease of coercivity with net moment. Finally, it has been found, that the saturation field of the patterned AFis is decreasing with larger aspect ratio and is asymptotically reaching the saturation field of the unpatterned films. The origin for this behavior for small aspect ratios can be found in the additional contribution of the stray field coupling of the two ferromagnetic layers within the AFi. Therefore the antiparallel alignment of the system is additionally favoured by the stray field coupling, depending basically on the demagnetization factor n_x vs. aspect ratio.

Acknowledgments

The authors wish to thank J. Bangert and G. Gieres for fruitful discussions, H. Mai and K. Rott for experimen-

tal support. Financial support of the German Ministry for Education and Research is gratefully acknowledged (Grant no. 13N8208).

References

- [1] M.K. Ho, C.H. Tsang, R.E. Fontana, S.S.P. Parkin, K.J. Carey, T. Pan, S. MacDonald, P.C. Arnett, and J.O. Moore, IEEE Trans. Magn. **37**, 1691 (2001)
- [2] H.A.M. van den Berg, J. Altmann, L. Bär, G. Gieres, R. Kinder, G. Rupp, M. Vieth, and J. Wecker, IEEE Trans. Magn. **35**, 2892 (1999)
- [3] M. Löhdorf, T. Duenas, M. Tewes, E. Quandt, M. Rührlig, and J. Wecker, Appl. Phys. Lett. **81**, 313 (2002)
- [4] W.J. Gallagher, S.S.P. Parkin, Y. Lu, X.P. Bian, A. Marley, K.P. Roche, R.A. Altman, S.A. Rishton, C. Jahnes, T.M. Shaw, and G. Xiao, J. Appl. Phys. **81**, 3741 (1997)
- [5] R. Richter, L. Bär, J. Wecker, and G. Reiss, Appl. Phys. Lett. **80**, 1291 (2002)
- [6] R.H. Koch, J.G. Deak, D.W. Abraham, P.L. Trouilloud, R.A. Altman, Y. Lu, W.J. Gallagher, R.E. Scheuerlein, K.P. Roche, and S.S.P. Parkin, Phys. Rev. Lett. **81**, 4512 (1998)
- [7] R.C. Sousa, Z. Zhang, and P.P. Freitas, J. Appl. Phys. **91**, 7700 (2002)
- [8] N. Tezuka, N. Koike, K. Inomata, and S. Sugimoto, J. Appl. Phys. **93**, 7441 (2003)
- [9] H.A.M van den Berg, W. Clemens, G. Gieres, G. Rupp, and M. Vieth, IEEE Trans. Magn. **32**, 4624 (1996)
- [10] N. Wiese, T. Dimopoulos, M. Rührlig, J. Wecker, H. Brückl, and G. Reiss, J. Magn. Magn. Mater. **290-291**, 1427 (2005)
- [11] N. Wiese, T. Dimopoulos, M. Rührlig, J. Wecker, H. Brückl, and G. Reiss, Appl. Phys. Lett. **85**, 2020 (2004)
- [12] D. Wang, C. Nordman, J. Daughton, Z. Qian, and J. Fink, IEEE Trans Magn **40**, 2269 (2004)
- [13] T. Dimopoulos, N. Wiese, G. Gieres, J. Wecker and M.D. Sacher, J. Appl. Phys. **96**, 6382 (2004)
- [14] D.W. Abraham, and Y. Lu, J. Appl. Phys. **98**, 023902 (2005)
- [15] for detailed specification of the NanoMOKE2™ system look at the website of Durham Magneto Optics Ltd., <http://durhammagnetooptics.com>
- [16] J.Z. Sun, J.C. Slonczewski, P.L. Trouilloud, D. Abraham, I. Bacchus, W.J. Gallagher, J. Hummel, Y. Lu, G. Wright, S.S.P. Parkin, and R.H. Koch, Appl. Phys. Lett. **78**, 4004 (2001)
- [17] A. Hubert, R. Schäfer, *Magnetic Domains, The Analysis of Magnetic Microstructures*, Springer (1998)
- [18] D. Meyners, H. Brückl, and G. Reiss, J. Appl. Phys. **93**, 2676 (2003)
- [19] The commercial available micromagnetic program (LLG Micromagnetics Simulator™) developed by M.R. Scheinfein was used, see <http://llgmicro.home.mindspring.com>